J Therm Anal Calorim (2016) 123:1281–1291
DOI 10.1007/s10973-015-5081-3

Synergistic effect of iron oxide modified carbon nanotubes on the thermal stability of silicone rubber under different atmospheres

Lu Bai[1] · Junping Zheng[1]

Received: 1 July 2015 / Accepted: 29 September 2015 / Published online: 15 October 2015

Abstract To investigate the synergistic effect and mechanism of γ-Fe_2O_3 modified carbon nanotubes (γ-Fe_2O_3–CNTs) on the thermal stability of silicone rubber (SR) under different atmospheres, a series of SR-based composites added with α-Fe_2O_3, γ-Fe_2O_3, CNTs and γ-Fe_2O_3–CNTs were prepared and subsequently investigated by Raman spectra, X-ray diffraction, thermogravimetric analysis and tensile testing before and after aging and swelling experiment. The results exhibited that γ-Fe_2O_3–CNTs had significant synergistic effect on the thermal stability of SR both under nitrogen and air atmosphere. Under nitrogen atmosphere, the depolymerization of SR was delayed greatly by γ-Fe_2O_3–CNTs in the whole temperature range. For example, T_{50} (the temperature at which 50 % degradation occurs) of γ-Fe_2O_3–CNTs/SR was 56.9 °C higher than that of neat SR. The synergistic effect is attributed to the nice combination of thermal conductivity of CNTs in the relatively low-temperature range and enhanced interfacial reaction of γ-Fe_2O_3 in the relatively high-temperature range. Under air atmosphere, the initial degradation temperature of γ-Fe_2O_3–CNTs/SR was greatly improved by about 50 °C. The synergistic effect is mainly proposed to include that CNTs and γ-Fe_2O_3 can promote each other to capture the free radicals and thereby terminate the thermo-oxidative degradation process significantly. Owing to the excellent antioxidant ability of γ-Fe_2O_3–CNTs, the degradation mechanism of its SR composite is changed completely.

Keywords Silicone rubber · Carbon nanotubes · Iron oxide · Thermal stability · Synergistic effect · Degradation atmosphere

Introduction

Silicone rubber (SR), the important synthetic rubber with excellent thermal stability, is widely used as an elastic material in high-temperature fields such as transportation, aerospace and defense industry [1–3]. With the rapid development of science and technology, a demand for high-performance silicone elastomer, especially for thermal resistant SR, has increased greatly [4, 5]. The thermal aging of SR is greatly influenced by oxygen. Depending on whether oxygen participates in the reactions, it can be divided into two different degradation mechanisms. The first mechanism is the depolymerization of SR backbone under oxygen-free atmosphere, and the second one is the complex conjunction of oxidation of side groups and degradation of SR backbone under air atmosphere [6–8].

As a simple and effective method to improve the thermal stability of SR, adding thermal resistant additives has been extensively studied. The metal oxide is one of the most popular additives to improve the thermo-oxidative stability of SR under air atmosphere. The mechanism is generally attributed to that the metal oxide can capture radicals generated in the oxidation reactions and thereby block the degradation process [9].

Since discovered by Iijima [10], carbon nanotubes (CNTs) have attracted enormous attention for the unique structure and outstanding mechanical, thermal and electronic properties

✉ Junping Zheng
jpzheng@tju.edu.cn

[1] Tianjin Key Laboratory of Composite and Functional Materials, School of Materials Science and Engineering, Tianjin University, Tianjin 300072, People's Republic of China

[11]. It is reported that CNTs also can improve the thermal stability of SR. Zhang thought that the CNTs filler's ability to suppress thermal degradation of SR might be attributed to barrier effects, as in the case of clay fillers, which could decrease the mobility of polymer [12]. Azizan' results indicated that CNTs could form a conductive network which facilitated the phonon transfer and leaded to high thermal conductivity, so that the thermal stability of the nanocomposites was improved [13].

In our previous work, we found that γ-Fe_2O_3 modified CNTs (γ-Fe_2O_3–CNTs) could remarkably improve the thermo-oxidative stability of SR nanocomposites and the effect was superior to CNTs, γ-Fe_2O_3, or a mixture of both at the same addition amount. This phenomenon was attributed to the synergistic effect of γ-Fe_2O_3 and CNTs [14, 15]. However, our previous work mainly focused on improving the actual performance of SR composites rather than studying the mechanism in depth, and thereby, plenty of reinforcing components including 40 phr (parts per hundreds of rubber) of fumed silica, 10 phr of hexamethyldisilazane and 2.6 phr of polyvinylsiloxane were added into the SR matrix. Obviously, the existence of these massive reinforcing components makes the SR composite system become much more complex and is bound to cause great obstruction to research in detail the synergistic effect and mechanism of γ-Fe_2O_3–CNTs on the thermal stability of SR. Hence, a new SR composite system as simple as possible that only contains the SR matrix, thermal resistant additives and curing agent is exceedingly necessary. In addition, taking into consideration the notable influence of oxygen on the thermal degradation process of SR, the comprehensive study of thermal depolymerization of SR composites under oxygen-free atmosphere which was hardly involved in the previous work can act as the contrast effectively to interpret the synergistic effect and mechanism of γ-Fe_2O_3–CNTs more deeply.

In this study, a series of SR-based nanocomposites filled with α-Fe_2O_3, γ-Fe_2O_3, CNTs and γ-Fe_2O_3–CNTs were prepared. By using Raman spectra, X-ray diffraction (XRD), thermogravimetric (TG) analysis, tensile testing and M_c (the average molecular weight between crosslinks) measurement, the synergistic effect and mechanism of γ-Fe_2O_3–CNTs on the thermal stability of SR under different atmospheres were investigated in detail.

Experimental

Materials

Methylvinyl silicone gum (110-2; Mn, 5.0×10^5–7.0×10^5; vinyl group content, 0.15–0.18 mol %; end-blocked with trimethylsiloxy groups ($(CH_3)_3Si$–) was purchased from Bluestar Chengrand Chemical Co. Ltd (Chengdu, China). Carboxylic CNTs (carboxyl ratio, 2.31 mass%; purity, >95 %; diameter, 20–40 nm; length, 1–2 μm) were purchased from Shenzhen Nanotech Port Co. Ltd China. 2,5-bis(tertbutylperoxy)-2,5-dimethylhexane(DBPMH) was a industrial product and used as obtained. Other reagents were all of analytical grade.

Preparation of γ-Fe_2O_3–CNTs

The process of preparation was the same as our previous work [14]. A typical procedure was as follows: 1.50 g of $Fe(NO_3)_3 \cdot 9H_2O$ was added into 200 mL of absolute ethanol and stirred until it was dissolved completely. This solution was added by 0.35 g of carboxylic CNTs, stirred and sonicated for 3 h. 0.08 g of sodium dodecylbenzenesulfonate was added into the solution, the mixture was stirred, and then, 24 mL of ammonia solution was added as a gelation agent and stirred. The mixture was filtered and washed by a large amount of deionized water and then vacuum-dried at 60 °C for 72 h. The calcination of this powder was performed at 600 °C in a muffle furnace under nitrogen atmosphere for 5 h and then annealed. The γ-Fe_2O_3 modified CNTs were obtained and named γ-Fe_2O_3–CNTs.

Preparation of α-Fe_2O_3, γ-Fe_2O_3 and the control CNTs

The preparing process α-Fe_2O_3 was the same as that of preparing γ-Fe_2O_3–CNTs without the existence of CNTs. To prepare γ-Fe_2O_3, α-Fe_2O_3 was calcined in a muffle furnace at 400 °C for 0.5 h under hydrogen atmosphere and was changed to Fe_3O_4. Then Fe_3O_4 was calcined in a muffle furnace at 300 °C for 3 h under air atmosphere and was changed to γ-Fe_2O_3. To be used as a control additive, carboxylic CNTs were also calcined at 600 °C in a muffle furnace under nitrogen atmosphere for 5 h and then annealed.

Preparation of SR-based composites

Materials were milled on a two-roll mill (SR-160B, Guangdong Zhanjiang Machinery Factory, China). 100 phr of silicone gum was encapsulated onto rollers. Then 3 phr of the prepared particles was added, respectively. After being milled uniformly, 0.7 phr of DBPMH was added. The mixture was cured in a stainless steel mold at 180 °C under a pressure of 10 MPa for 10 min and postcured at 200 °C for 4 h under ambient pressure for crosslinking.

Thermal aging and thermo-oxidative aging experiments of SR-based composites

The thermal aging experiment and thermo-oxidative aging experiment of SR-based composites were carried out in a

muffle furnace at 300 °C for 12 h under nitrogen and air atmosphere, respectively.

Measurements

Raman spectra were recorded on a DXR Raman spectrometer with a 532-nm laser in the range of 500–2000 cm^{-1} at room temperature.

XRD measurement of γ-Fe_2O_3/SR samples before and after aging 5 h at 300 °C under nitrogen and air atmosphere, respectively, in a muffle furnace was carried out using an X-ray diffractometer (Rigaku DMAX-RC, Japan) with Cu Kα radiation ($\lambda = 0.15418$ nm) under a generator voltage of 45 kV and a generator current of 180 mA at room temperature, scanning from 20° to 80° at a rate of 2° min^{-1}.

TG analysis of SR-based composites was performed using a STA449F3 (Netzsch, Germany) instrument. About 10 mg of sample cut as small pieces was heated in an Al_2O_3 crucible under nitrogen atmosphere from ambient temperature to 800 °C at a heating rate of 10 °C min^{-1} and under air atmosphere from ambient temperature to 650 °C at the same heating rate.

The tensile testing was performed on a universal testing machine (M350-20KN, Testometric, UK) at a 500 mm min^{-1} crosshead speed at room temperature. The dumbbell-shaped specimens were obtained from vulcanized sheet. At least three specimens were tested for each sample, and the mean value was reported.

The M_c of SR composites was measured by swelling experiment [16]. A certain amount of sample was immersed in 100 mL toluene for 72 h at 30 °C to attain equilibrium swelling, and after the equilibrium swelling, the sample was taken out, and the solvent was blotted from the surface of the sample and weighted immediately. M_c was calculated by the Flory-French Eq. (1):

$$M_c = \frac{-\rho_2 V_0 \phi^{\frac{1}{3}}}{\ln(1-\phi) + \phi + \chi\phi^2} \quad (1)$$

where V_0 is the molar volume of the solvent; χ is Flory–Huggins interaction parameter between polymer and solvent, here 0.465; φ is the volume fraction of SR in the swelling rubber, which can be obtained through Eq. (2):

$$\phi = \frac{W_1/\rho_2}{(W_2 - W_1)/\rho_1 + W_1/\rho_2} \quad (2)$$

where ρ_1 and ρ_2 are the densities of toluene and SR, respectively; W_1 is the initial mass of SR composite, and W_2 is the mass of swollen SR composite.

Results and discussion

Characterization of the influence of metal oxide coating on CNTs

The results of Raman spectra of CNTs and γ-Fe_2O_3–CNTs are shown in Fig. 1. The strong peaks at about 1345 and 1572 cm^{-1} observed both on the spectra of CNTs and γ-Fe_2O_3–CNTs can be assigned to the D-band and the G-band of multiwall CNTs, respectively [17]. The D-band is related to local defects that originate from structural imperfections, and the G-band is caused by the tangential C–C stretching vibration that is associated with the ordered sp^2 hybridized carbon network [18]. Generally, the ratio of the Raman intensities of the D- and G-band (I_D/I_G) is used as a criterion to estimate the concentration of structural defects in CNTs [19]. The calculated values of I_D/I_G for CNTs and γ-Fe_2O_3–CNTs are 1.164 and 1.359, respectively. The result is consistent with the previous researches [20, 21] that the metal oxide coating can damage the order of graphite layers of CNTs and thereby increase the concentration of defects.

The crystal transformation of γ-Fe_2O_3 under different atmospheres

The XRD measurement was employed to investigate the crystal transformation of γ-Fe_2O_3 nanoparticles in γ-Fe_2O_3/SR composite samples after aging 5 h at 300 °C under nitrogen and air atmosphere, respectively. Figure 2 illustrates the XRD patterns of (a) γ-Fe_2O_3/SR before aging, (b) γ-Fe_2O_3/SR after aging under nitrogen and (c) γ-Fe_2O_3/

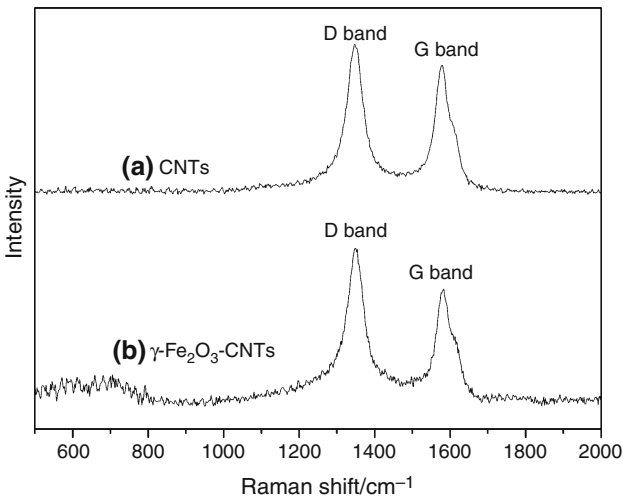

Fig. 1 Raman spectra of (*a*) CNTs and (*b*) γ-Fe_2O_3–CNTs

SR after aging under air. The diffraction peaks in Fig. 2a at $2\theta = 30.1°$, 35.4°, 37.1°, 43.1°, 57.0° and 62.6° can be attributed to (220), (311), (222), (400), (511) and (440) planes of γ-Fe_2O_3, respectively. Figure 2b is nearly the same as Fig. 2a, showing that the crystal form of γ-Fe_2O_3 did not change after aging under nitrogen atmosphere. Figure 2c not only has diffraction peaks corresponding to planes of γ-Fe_2O_3 mentioned above, but also has obvious diffraction peaks at $2\theta = 24.1°$, 33.2°, 39.3°, 49.5° (marked with Δ) which are assigned to (012), (104), (006) and (024) planes of α-Fe_2O_3, respectively. This shows that after thermal aging under air atmosphere, part of γ-Fe_2O_3 was converted into α-Fe_2O_3.

The results of XRD indicate that the crystalline structure of γ-Fe_2O_3 remains the same after aging under nitrogen atmosphere, providing a prerequisite to analyze the role of γ-Fe_2O_3 in improving the thermal stability of SR in oxygen-free atmosphere. In addition, as reported in our previous work [14], the crystal transformation of γ-Fe_2O_3 in thermo-oxidative process can enhance the antioxidant effect of γ-Fe_2O_3 and thereby improve the thermal stability of SR under air atmosphere.

Thermal degradation of SR-based composites under nitrogen atmosphere

TG and differential thermogravimetry (DTG) curves of SR-based composites under nitrogen atmosphere are shown in Figs. 3 and 4, respectively. Meanwhile, the details of mass loss data, including the onset degradation temperature T_{onset} (defined as the temperature for 1 % mass loss), characteristic temperatures T_5, T_{20} and T_{50} (the temperature at which 5, 20 and 50 % degradation occurs, respectively), the peak temperature T_p (the temperature at the peak of DTG curve) and final residue (defined as the mass remaining at 750 °C under nitrogen atmosphere), are also summarized in Table 1.

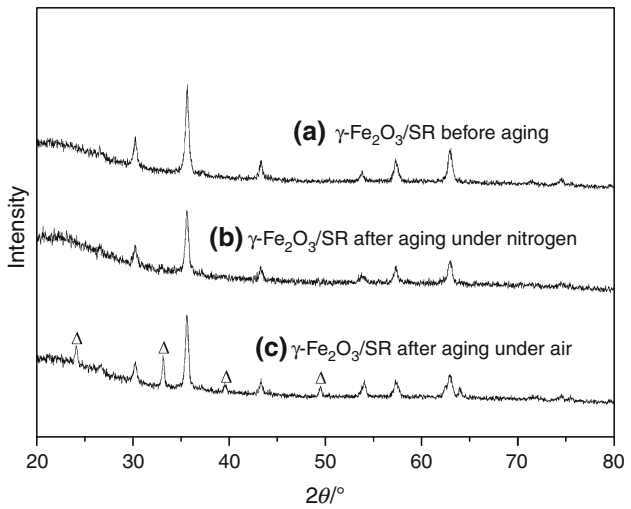

Fig. 2 XRD patterns of γ-Fe_2O_3/SR composite before and after aging 5 h at 300 °C under nitrogen and air atmosphere, respectively: (*a*) γ-Fe_2O_3/SR before aging; (*b*) γ-Fe_2O_3/SR after aging under nitrogen; (*c*) γ-Fe_2O_3/SR after aging under air

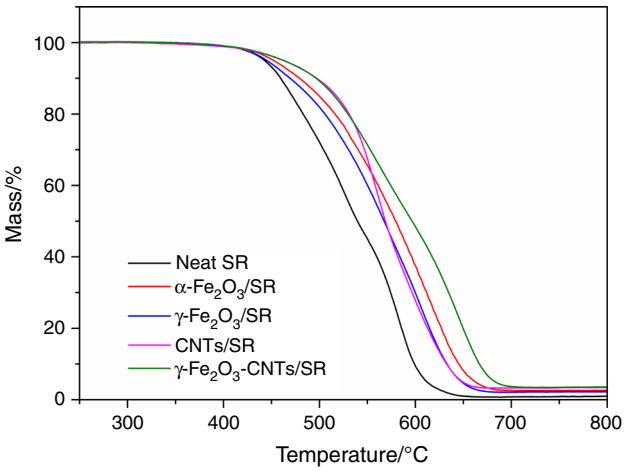

Fig. 3 TG curves for SR-based composites at constant heating rate 10 °C min^{-1} under nitrogen atmosphere

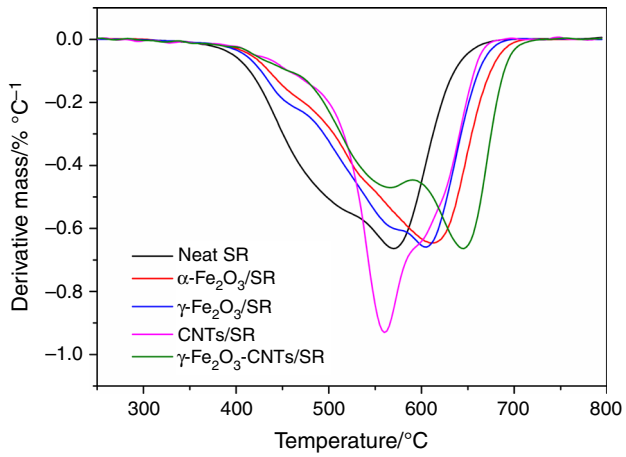

Fig. 4 DTG curves for SR-based composites at constant heating rate 10 °C min^{-1} under nitrogen atmosphere

Obviously, only a main degradation stage can be observed in the TG curve of neat SR under nitrogen atmosphere. Depending on the type of terminal groups (trimethylsilyl) as well as the low concentration of external impurities, we believe that the depolymerization is just dominated by the random main chain scission mechanism [7, 22, 23], which can be expounded in detail that SR thermally decomposes to cyclic oligomers through Si–O bond scission in a chain-folded cyclic conformation energetically favored by overlapping of empty silicon d-orbitals with orbitals of oxygen and carbon atoms [6]. Moreover, the formation of intramolecular cyclic transition state,

Table 1 The characteristic degradation results obtained from TG and DTG curves under nitrogen atmosphere

Sample	T_{onset}/°C	T_5/°C	T_{20}/°C	T_{50}/°C	T_p/°C T_p^1, T_p^2	Final residue at 750 °C/%
Neat SR	399.2	442.8	459.5	539.3	568.1	0.99
α-Fe_2O_3/SR	402.0	452.3	479.2	579.1	608.7	1.72
γ-Fe_2O_3/SR	401.7	445.2	469.1	566.7	605.7	2.21
CNTs/SR	401.9	462.4	497.6	568.8	560.1	3.59
γ-Fe_2O_3–CNTs/SR	402.3	462.3	496.1	596.2	567.5, 645.0	3.56

affected by the mobility of molecules, is the rate-determining step of the depolymerization process [8].

The shapes of TG and DTG curves of α-Fe_2O_3/SR can be found similar to those of neat SR, respectively, indicating that the thermal degradation mechanism of α-Fe_2O_3/SR under nitrogen atmosphere was not changed greatly. However, the depolymerization of α-Fe_2O_3/SR was delayed compared with neat SR. For example, T_5, T_{20}, T_{50} and T_p of α-Fe_2O_3/SR were increased by 9.5, 19.7, 39.8 and 40.6 °C, respectively. The influence of γ-Fe_2O_3 is similar to α-Fe_2O_3. Yet, the improvement of T_5, T_{20}, T_{50} and T_p of γ-Fe_2O_3/SR (2.4, 9.6, 27.4 and 37.6 °C, respectively) in comparison with neat SR is slightly less than those of α-Fe_2O_3/SR, respectively.

Likely due to the bonding of rubber chains to particle surfaces, iron oxide can form an interfacial reaction with SR matrix [24]. Similar to physical crosslinking, the interfacial reaction can increase the crosslinking density, hinder the formation of cyclic transition conformation and thereby delay the depolymerization of SR. The diverse effects of α-Fe_2O_3 and γ-Fe_2O_3 are proposed to result from the difference of crystal structure, which can aspect the arrangement of Fe atoms in particle surfaces.

TG and DTG curves of CNTs/SR are different from neat SR and can be divided into two stages. In the relatively low-temperature range (below 530 °C), CNTs/SR has the highest thermal stability among all samples. For example, CNTs/SR has the highest T_{20} that is 38.1, 18.4, 28.5 and 1.5 higher than those of neat SR, α-Fe_2O_3/SR, γ-Fe_2O_3/SR and γ-Fe_2O_3–CNTs/SR, respectively. However, when the temperature threshold (about 530 °C) is reached, an abrupt acceleration of the mass loss is observed, indicating that CNTs/SR undertakes a rapid degradation process in the second stage.

According to literatures, we propose that CNTs have two main aspects of effects on degradation of SR under nitrogen atmosphere. First, the barrier effect of CNTs can decrease the mobility of polymer as in the case of clay fillers and suppress thermal degradation of SR [12]. Second, owing to the excellent thermal conductivity, CNTs can form an effective thermal conducting network in matrix, which can eliminate the local overheating of SR (the excessive heat quenching ability [25]) and thus delay the thermal degradation [14]. In the low-temperature range, the thermal conductivity of CNTs is extremely efficacious and makes CNTs/SR have the best thermal stability. With the ambient temperature increasing to the critical value, the thermal conducting effect of CNTs becomes ineffective quickly, which can be attributed to the rapid decline of thermal conductivity of CNTs as temperature increases [26, 27] along with the destruction of the thermal conducting nanotube network [28]. Yet, with the existence of the barrier effect, the thermal stability of CNTs/SR is still higher than that of neat SR.

Degradation of γ-Fe_2O_3–CNTs/SR gives results much different from neat SR and other SR composites. Two overlapped peaks located in 567.5 and 645.0 °C, respectively, can be found in the DTG curve of γ-Fe_2O_3–CNTs/SR. From Fig. 3, it can be seen clearly that γ-Fe_2O_3–CNTs/SR has the most outstanding thermal stability among all samples. Take T_{50} as an example to explain. Compared to those of neat SR, α-Fe_2O_3/SR, γ-Fe_2O_3/SR and CNTs/SR, T_{50} of γ-Fe_2O_3–CNTs/SR are raised by 56.9, 17.1, 29.5 and 27.4 °C, respectively.

As analyzed above, though γ-Fe_2O_3 and CNTs both can improve the thermal stability of SR under nitrogen, the mechanism is very different. T_p^1 and T_p^2 (the temperature at the first and the second peak of DTG curve, respectively) are close to T_p of CNTs/SR and γ-Fe_2O_3/SR, respectively, indicating that the first and second DTG peaks should be attributed to the CNTs and γ-Fe_2O_3, respectively. In particular, T_p^2 of γ-Fe_2O_3–CNTs/SR is increased by about 40 °C by contrast of T_p of γ-Fe_2O_3/SR, showing that the effect of γ-Fe_2O_3 was greatly enhanced. Just as reported in our previous work [14, 15], CNTs could greatly reduce the particle size of γ-Fe_2O_3 (the γ-Fe_2O_3 on CNTs has a particle size of about 10 nm, while the single γ-Fe_2O_3 has a particle size of about 80 nm) and inhibit the aggregation of nanoparticles, so that the interaction between iron oxide particles and matrix could be improved significantly.

Considering that the amount of γ-Fe_2O_3 and CNTs in γ-Fe_2O_3–CNTs is less than that of single γ-Fe_2O_3 and CNTs,

respectively, we can surely infer that it is the synergistic effect of respective effects of γ-Fe_2O_3 and CNTs. More accurately, the synergistic effect is attributed to the nice combination of thermal conductivity of CNTs in the relatively low-temperature range and enhanced interfacial reaction of γ-Fe_2O_3 in the relatively high-temperature range.

Thermo-oxidative degradation of SR-based composites under air atmosphere

The TG and DTG curves of SR-based composites under air atmosphere are presented in Figs. 5 and 6, respectively. Also, the characteristic degradation results obtained from the TG and DTG curves are listed in Table 2.

Thermo-oxidative degradation of SR-based composites with the presence of air gives results much different from the thermal degradation under nitrogen atmosphere. As for neat SR, T_{onset} was largely reduced by about 50 °C in comparison with that of thermal degradation under nitrogen atmosphere, due to the catalysis and acceleration effects of oxygen on SR degradation [6]. In addition, two major degradation peaks can be found in the DTG curves under air atmosphere, indicating the existence of two overlapping stages in the overall degradation process. According to several previous articles [22, 23], the first degradation stage (mass loss about 10 %) which occurs in the relatively low-temperature range (from 340 to 400 °C approximately) is likely due to the thermo-oxidative effect, involving the thermo-oxidative process of the methyl side groups in SR chains and the oxidative crosslinking reaction (shown in Fig. 7). The second degradation stage (mass loss about 50 %) predominating in the relatively high-temperature range (from 400 to 550 °C approximately) can be

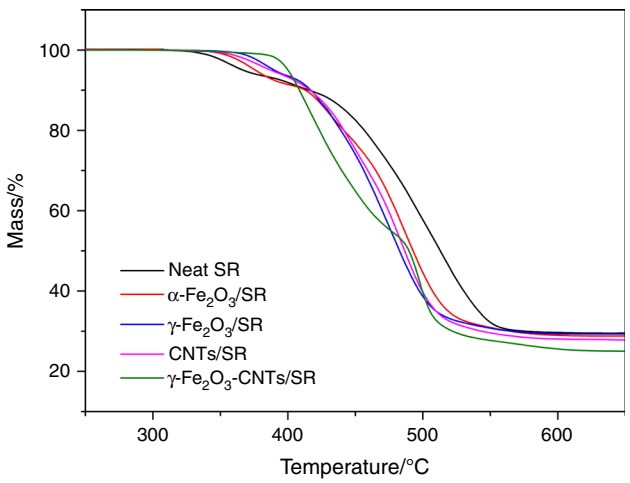

Fig. 5 TG curves for SR-based composites at constant heating rate 10 °C min^{-1} under air atmosphere

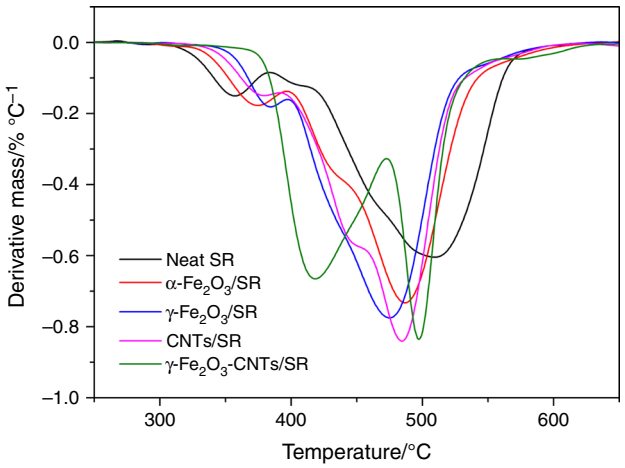

Fig. 6 DTG curves for SR-based composites at constant heating rate 10 °C min^{-1} under air atmosphere

attributed to the thermal depolymerization of SR backbone as in nitrogen [6, 23].

Because of the nonnegligible existence of thermo-oxidative effect, the degradation behavior of SR under air atmosphere is much more complicated than that under nitrogen atmosphere. On the one hand, the thermal oxidation of SR occurring mainly in the relatively low-temperature range can catalyze degradation to cyclic oligomers [6, 22, 23], likely due to the acceleration effect of free radicals generated in oxidation on the depolymerization, so that the degradation will occur in a lower temperature. On the other hand, the oxidative crosslinking can largely decrease the mobility of SR chain and thereby hinder further splitting of cyclic oligomers. In other words, it improves the stability of SR and suppresses the depolymerization mainly occurring in the relatively high-temperature range. To sum up, the complex competitive relationship between thermo-oxidative effect and thermal depolymerization reaction provides a prerequisite for us to analyze the role of additives in influencing the thermo-oxidative degradation behaviors of SR-based composites under air atmosphere.

As for SR composites, the degradation behaviors of α-Fe_2O_3/SR, γ-Fe_2O_3/SR and CNTs/SR are similar to that of neat SR, meaning that degradation mechanism of the four samples can be regarded as the same. It is obvious that the first degradation stage of α-Fe_2O_3/SR, γ-Fe_2O_3/SR and CNTs/SR was delayed compared to that of neat SR. For example, T_{onset} of α-Fe_2O_3/SR, γ-Fe_2O_3/SR and CNTs/SR was improved by 11.1, 27.5 and 19.4 °C, respectively. Also, T_p^1 of α-Fe_2O_3/SR, γ-Fe_2O_3/SR and CNTs/SR, which corresponded to the oxidation of side methyl groups, was increased by 17.5, 26.9 and 21.3 °C, respectively, by contrast of that of neat SR. However, in the second degradation stage, all of α-Fe_2O_3/SR, γ-Fe_2O_3/SR and CNTs/SR exhibited a trend of accelerated degradation

Table 2 The characteristic degradation results obtained from TG and DTG curves under air atmosphere

Sample	T_{onset}/°C	T_5/°C	T_{20}/°C	T_{50}/°C	T_p/°C T_p^1, T_p^2	Final residue at 650 °C/%
Neat SR	337.5	367.4	456.4	515.9	357.5, 510.0	29.5
α-Fe_2O_3/SR	348.6	376.3	441.4	493.1	375.0, 487.5	28.8
γ-Fe_2O_3/SR	365.0	390.5	439.1	482.8	384.4, 474.3	28.9
CNTs/SR	356.9	387.5	441.6	486.5	378.8, 482.1	27.8
γ-Fe_2O_3–CNTs/SR	387.1	399.1	422.8	515.0	419.0, 496.8	25.0

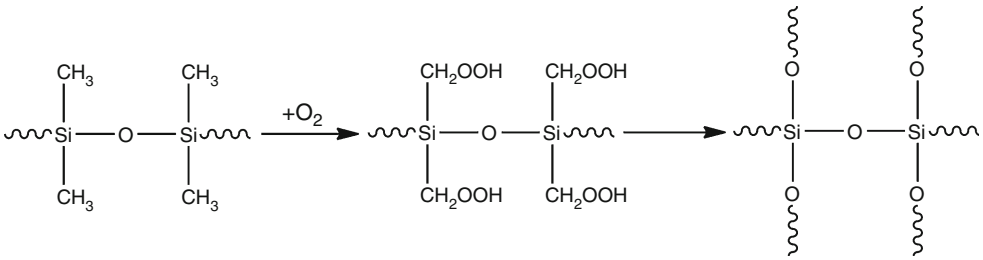

Fig. 7 The oxidative crosslinking reaction

compared with neat SR. For example, T_{50} of α-Fe_2O_3/SR, γ-Fe_2O_3/SR and CNTs/SR is 22.8, 33.1 and 29.4 °C lower than that of neat SR, respectively. Besides, T_p^2 of α-Fe_2O_3/SR, γ-Fe_2O_3/SR and CNTs/SR, which correspond to the degradation of backbone, is 22.5, 35.7 and 27.9 °C lower than that of neat SR, respectively.

Oxidation is likely to proceed through peroxidation mechanism which leads to the generation of free radicals and oxidation products [6]. As for α-Fe_2O_3 and γ-Fe_2O_3, their antioxidant effect for SR is mainly due to that Fe^{3+} can capture radicals produced in oxidation and thereby block the proceeding of oxidative reactions [9, 14]. The improvement of T_{onset} of γ-Fe_2O_3/SR by contrast of neat SR is higher than that of α-Fe_2O_3/SR, showing that γ-Fe_2O_3 is a more effective thermo-oxidative resistant additive. It has been confirmed by the XRD results (Fig. 2) that after aging under air atmosphere, γ-Fe_2O_3 nanoparticles were partly converted to α-Fe_2O_3. γ-Fe_2O_3 is much more unstable than α-Fe_2O_3. The change in crystalline form from γ to α needs the existence of oxygen [29, 30]. In a word, γ-Fe_2O_3 not only can scavenge free radicals, but also create a hypoxic environment around γ-Fe_2O_3 particles [14]. Therefore, the antioxidant effect of γ-Fe_2O_3 is better than α-Fe_2O_3.

As for the degradation of CNTs/SR under air atmosphere, we believe that the radical scavenging ability of CNTs should be more dominant than the thermal conducting effect and barrier effects as mentioned in the TG analysis of CNTs/SR under nitrogen atmosphere, which can be proved by the similar antioxidant effect between CNTs and other two certain free radical scavenging agents (γ-Fe_2O_3 and α-Fe_2O_3). Apropos of the radical scavenging ability of CNTs, as stated in the previous research [31], the localized states of CNTs due to lattice defects (e.g., vacancies, dangling bonds, OH and CO attachments) are acceptor-like [32, 33]. The presence of acceptor-like electronic properties in CNTs is effective to trap free radicals and thereby terminate the oxidation process.

However, the adding of antioxidant additives is really a double-edged sword. It can not only restrain the oxidation of side methyl groups in the first degradation stage, but also inhibit the oxidative crosslinking reaction which can delay the depolymerization of SR. So the degradation of SR backbone of SR composites in the second stage is promoted. Meanwhile, the sequence of T_{onset} as well as T_p^1 of four samples from low to high is neat SR, α-Fe_2O_3/SR, CNTs/SR and γ-Fe_2O_3/SR, while that of T_p^2 is completely opposite, proving that the greater the inhibition of oxidation in the first degradation stage is, the greater the promotion of the SR backbone in the second degradation stage is.

As for γ-Fe_2O_3–CNTs/SR, it seems extremely strange that in the first degradation stage there is a noticeably large mass loss which is about 50 % and much higher than those of other four samples (about 10 %). The mass loss is so great that it cannot be attributed to the thermal oxidation of side methyl groups of SR as others. Therefore, the different degradation behavior of γ-Fe_2O_3–CNTs/SR means a new degradation mechanism different from neat SR and other three SR composites.

Compared with neat SR, T_{onset} of γ-Fe_2O_3–CNTs/SR was greatly increased by 49.6 °C, which is much higher

than those of other SR composites added with α-Fe_2O_3, γ-Fe_2O_3 and CNTs. The result shows that γ-Fe_2O_3–CNTs is an excellent thermal resistant additive of SR under air atmosphere. Considering that the amount of γ-Fe_2O_3 and CNTs in γ-Fe_2O_3–CNTs is, respectively, less than that of single γ-Fe_2O_3 and CNTs, we can infer that it is not a simple accumulation, but a synergistic effect of CNTs and γ-Fe_2O_3.

When analyzing the synergistic effect of γ-Fe_2O_3–CNTs under nitrogen atmosphere, we have pointed out that CNTs can enhance the interfacial reaction of γ-Fe_2O_3 and SR matrix. As for the thermo-oxidative degradation of γ-Fe_2O_3–CNTs/SR under air atmosphere, due to the new emergence of nonnegligible thermo-oxidative effect which can be regarded as a series of complex free radical reactions, the radical scavenging ability of γ-Fe_2O_3 and CNTs which is generally ignorable in the thermal depolymerization of SR under nitrogen atmosphere should be focused on intensively. Therefore, except for the effects under nitrogen atmosphere, we propose that the synergistic effect under air atmosphere also includes: (1) Because of the high electrical conductivity, CNTs can act as an electron tunnel [34] which can facilitate the electron of the iron oxide during the radical scavenging transfer and speed up the scavenging. (2) The unique structure and properties of CNTs can influence the apparent Fermi level of metal oxide particles and narrow the band gap [35], so that the activity of the metal oxide particles is enhanced. (3) The metal oxide coating can increase the concentration of defects and thereby further enhance the radical accepting capacity of the CNTs [36].

Considering that T_{onset} of γ-Fe_2O_3–CNTs/SR under air atmosphere is close to that of γ-Fe_2O_3–CNTs/SR under nitrogen atmosphere (387.1 vs. 402.3 °C), we propose that the temperature has reached the threshold of depolymerization of SR backbone and the large mass loss just results from the degradation of SR backbone. Due to the excellent antioxidant effect of γ-Fe_2O_3–CNTs, the oxidation of side methyl groups as well as the oxidative crosslinking reaction is suppressed significantly, so that the mass loss does not start until the temperature reaches the threshold of SR backbone depolymerization.

From the result that the γ-Fe_2O_3–CNTs/SR sample finally degraded to considerable amount of stable residue, we can know that the oxidation of side methyl groups as well as the oxidative crosslinking reaction could not be inhibited permanently and took place in the end. In addition, the degradation rate of the second stage is even larger than that of the first degradation stage. Therefore, a reliable inference can be made that the second degradation stage of γ-Fe_2O_3–CNTs/SR is the combination of depolymerization of SR backbone and oxidation of side methyl groups as γ-Fe_2O_3–CNTs particles have lost the excellent antioxidant effect in the excessively high temperature. However, this kind of failure phenomenon of additive is not observed in the TG curve of CNTs/SR though both the two additives are derivatives of primary carboxylic CNTs.

In order to further understand the failure cause of γ-Fe_2O_3–CNTs particles, TG analysis of γ-Fe_2O_3–CNTs and pure CNTs under air atmosphere was taken and the results are shown in Fig. 8. Comparing Fig. 5 with Fig. 8, we can find that pure CNTs can remain stable below 600 °C, at which the degradation of SR under air atmosphere has finished entirely. Therefore, the oxidation of pure CNTs has little effect on the thermo-oxidative degradation of CNTs/SR composite. However, it is interesting to find that γ-Fe_2O_3–CNTs particles have a much lower onset temperature (about 400 °C) to lose mass. As shown in the analysis of Raman spectra (Fig. 1), the metal oxide coating can increase the concentration of defects, which are more likely to be oxidized. So the oxidation of CNTs is promoted. When the temperature reaches about 500 °C, the CNTs in γ-Fe_2O_3–CNTs particles have been destroyed fiercely by oxidation so that γ-Fe_2O_3–CNTs will lose the excellent antioxidant effect and the oxidation of SR will occur.

Mechanical properties of SR-based composites

The results of mechanical properties are presented in Fig. 9 and Fig. 10. As shown in Fig. 9, the tensile strength of all composites before aging is about 0.3 MPa and slightly larger than that of neat SR in general. After aging under nitrogen atmosphere, the tensile strength of all samples decreased by about 30 %. After aging under air atmosphere, the mechanical properties of neat SR, α-Fe_2O_3/SR and γ-Fe_2O_3/SR were too weak to be detected by the testing machine. The tensile strength of CNTs/SR and γ-

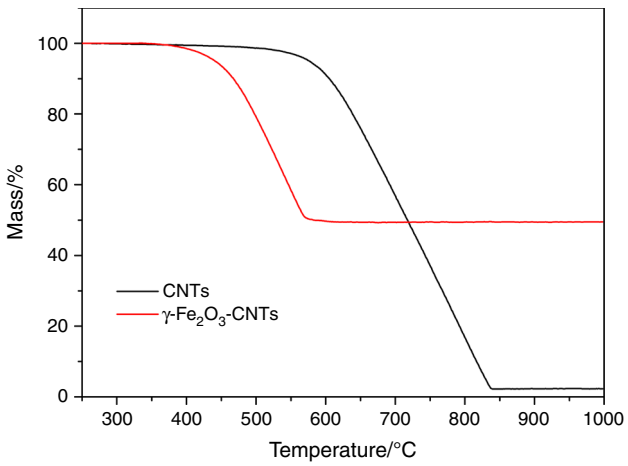

Fig. 8 TG curves for CNTs and γ-Fe_2O_3–CNTs particles at constant heating rate 10 °C min^{-1} under air atmosphere

Fe_2O_3–CNTs/SR is similar, accounting for about 60 % of the tensile strength before aging.

As shown in Fig. 10, the elongation at break of all SR composites before aging is close and slightly larger than that of neat SR in general. After aging under nitrogen atmosphere, the elongation at break of all SR samples was greatly increased and neat SR had the highest value. After aging under air atmosphere, the elongation at break of CNTs/SR decreased to about 60 %. It seems quite abnormal that the elongation at break of γ-Fe_2O_3–CNTs/SR was improved greatly and the value was close to the result under nitrogen atmosphere.

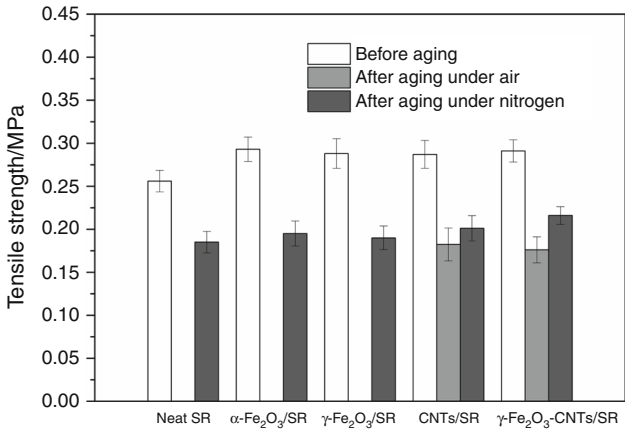

Fig. 9 Tensile strength of SR-based composites before and after thermal aging under nitrogen and air atmosphere, respectively

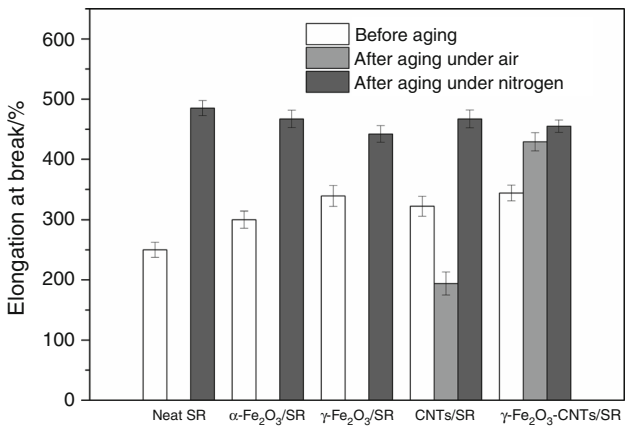

Fig. 10 Elongation at break of SR-based composites before and after thermal aging under nitrogen and air atmosphere, respectively

As mentioned above, the thermal aging under nitrogen atmosphere will result in degradation of SR backbone and generation of cyclic oligomers. So the sample will become softer, meaning a lower tensile strength and a higher elongation at break. The thermal resistant additives can delay the degradation of SR and thus improve the mechanical properties of SR after aging under nitrogen atmosphere to some extent. The thermal aging under air atmosphere is very complex. As for neat SR, because of the existence of oxidative crosslinking, the crosslinking density will be increased largely so that the sample will become much brittler. The same as neat SR, both α-Fe_2O_3/SR and γ-Fe_2O_3/SR became too brittle to be detected by the testing machine after aging under air atmosphere. CNTs/SR still remained mechanical properties to some extent, but both the tensile strength and elongation at break decreased largely. This result shows that the thermal aging process of CNTs/SR under air atmosphere is still dominated by the oxidative crosslinking. However, after aging under air atmosphere, the elongation at break of γ-Fe_2O_3–CNTs/SR was increased largely, similar to the aging result under nitrogen atmosphere. This indicates that the oxidative crosslinking was almost inhibited completely and the thermal aging of γ-Fe_2O_3–CNTs/SR under air atmosphere was dominated by the degradation of SR backbone. Considering that the aging temperature (300 °C) should be classified as a relatively low temperature as mentioned in the TG analysis under air atmosphere, the results also indirectly confirm the analysis of TG data that the first mass loss stage of γ-Fe_2O_3–CNTs/SR under air atmosphere is the degradation of SR backbone.

M_c measurement

In order to confirm the inferences of thermal aging mechanisms mentioned in the analysis of mechanical

Table 3 M_c of SR-based composites before and after aging 12 h at 300 °C under nitrogen and air atmosphere, respectively

Sample	M_c		
	Before aging	After aging under nitrogen	After aging under air
Neat SR	8965 ± 135	14,175 ± 147	5038 ± 194
α-Fe_2O_3/SR	8059 ± 137	13,575 ± 197	5446 ± 158
γ-Fe_2O_3/SR	8603 ± 248	14,009 ± 219	6073 ± 166
CNTs/SR	8204 ± 183	11,900 ± 251	5612 ± 201
γ-Fe_2O_3–CNTs/SR	8037 ± 164	12,766 ± 184	11,920 ± 245

properties, the M_c measurement of samples before and after aging 12 h at 300 °C under nitrogen and air atmosphere, respectively, was taken subsequently. The results are listed in Table 3.

M_c is an important structural parameter which can indicate the degree of crosslinking of vulcanizates. The higher the crosslinking density of vulcanizate is, the smaller the M_c is [16]. Oxidative crosslinking will increase the crosslinking density, while the degradation of SR backbone which can shorten the length of SR molecules will reduce the crosslinking density. From Table 3, we can find that before aging, all samples have a close M_c around 8000. After aging under nitrogen atmosphere, the M_c of all five samples is largely increased to about 13,000, proving that the main degradation mechanism of all samples is the depolymerization of SR backbone. After aging under air atmosphere, the M_c of neat SR, α-Fe_2O_3/SR, γ-Fe_2O_3/SR and CNTs/SR all decrease to about 5500, showing that the thermo-oxidative effect along with the oxidative crosslinking is the dominant mechanism. However, the M_c of γ-Fe_2O_3–CNTs/SR sample after aging under air atmosphere is increased significantly to 11,920 and nearly the same as the result obtained under nitrogen atmosphere, indicating that the aging process of γ-Fe_2O_3–CNTs/SR under air atmosphere is really dominated by the thermal depolymerization mechanism as analyzed above.

Conclusions

In this work, a series of SR composites added with α-Fe_2O_3, γ-Fe_2O_3, CNTs and γ-Fe_2O_3–CNTs were prepared. Raman spectra, TG analysis, XRD, tensile testing before and after aging and M_c measurement were used to investigate the synergistic effect and mechanism of γ-Fe_2O_3–CNTs on the thermal stability of SR under different atmospheres. The results exhibited that γ-Fe_2O_3–CNTs had significant synergistic effect on the thermal stability of SR both under nitrogen and air atmosphere. Under nitrogen atmosphere, γ-Fe_2O_3–CNTs could delay the depolymerization of SR in the whole temperature range greatly. Compared to that of neat SR, T_{50} of γ-Fe_2O_3–CNTs/SR was largely improved by 56.9 °C. The synergistic effect is attributed to the combination of thermal conductivity of CNTs in the relatively low-temperature range and enhanced interfacial reaction of γ-Fe_2O_3 in the relatively high-temperature range. Under air atmosphere, the effects of γ-Fe_2O_3–CNTs/SR were complex. Compared with neat SR, T_{onset} of γ-Fe_2O_3–CNTs/SR was increased by 49.6 °C, demonstrating the noticeable existence of synergistic effect which could enhance the antioxidant effect of the additive greatly. CNTs and γ-Fe_2O_3 can promote each other to capture the free radicals and thereby terminate the thermo-oxidative degradation process significantly. The oxidation was inhibited so strongly that the thermal degradation process of γ-Fe_2O_3–CNTs/SR under air atmosphere was completely reversed in comparison of neat SR and α-Fe_2O_3/SR, γ-Fe_2O_3/SR, CNTs/SR composites.

Acknowledgements The authors wish to thank the National Natural Science Foundation of China (Grant No. 51273143) for supporting this research.

References

1. Miwa M, Takeno A, Hara K, Watanabe A. Volume fraction and temperature dependence of mechanical properties of silicone rubber particulate/epoxy blends. Composites. 1995;26:371–7.
2. Liu L, Zhuo J, Chen X, Jiao C, Li S, Gu Y. Influence of ferric hydroxide on smoke suppression properties and combustion behavior of intumescent flame retardant silicone rubber composites. J Therm Anal Calorim. 2015;119:487–97.
3. Ghadir M, Zimonyi E, Nagy J. Thermal investigation of silicone rubber containing imide-siloxane copolymers. J Therm Anal Calorim. 1994;41:1019–29.
4. Wang L, Wang X, Li Y. Relation between repeated uniaxial compressive pressure and electrical resistance of carbon nanotube filled silicone rubber composite. Compos Part A Appl Sci Manuf. 2012;43:268–74.
5. Genovese A, Shanks RA. Fire performance of poly(dimethyl siloxane) composites evaluated by cone calorimetry. Compos Part A Appl Sci Manuf. 2008;39:398–405.
6. Camino G, Lomakin SM, Lazzari M. Polydimethylsiloxane thermal degradation Part 1. Kinetic aspects. Polymer. 2001;42:2395–402.
7. Rybiński P, Żukowski W, Bradło D. Influence of cenosphere particles on thermal properties composites of silicon rubber. J Therm Anal Calorim. 2015;. doi:10.1007/s10973-015-4829-0.
8. Thomas TH, Kendrick TC. Thermal analysis of polysiloxanes. II. Thermal vacuum degradation of polysiloxanes with different substituents on silicon and in the main siloxane chain. J Polym Sci, Part A: Polym Chem. 1970;8:1823–30.
9. Su Z. Interfacial reaction of stannic oxide in silicone rubber at 300°C. J Appl Polym Sci. 1999;73:2779–81.
10. Iijima S. Helical microtubules of graphitic carbon. Nature. 1991;354:56–8.
11. Baughman RH, Zakhidov AA, de Heer WA. Carbon nanotubes–the route toward applications. Science. 2002;297:787–92.
12. Katihabwa A, Wang W, Jiang Y, Zhao X, Lu Y, Zhang L. Multi-walled carbon nanotubes/silicone rubber nanocomposites prepared by high shear mechanical mixing. J Reinf Plast Compos. 2011;30:1007–14.
13. Norkhairunnisa M, Azizan A, Mariatti M, Ismail H, Sim LC. Thermal stability and electrical behavior of polydimethylsiloxane nanocomposites with carbon nanotubes and carbon black fillers. J Compos Mater. 2012;46:903–10.
14. Li H, Tao S, Huang Y, Su Z, Zheng J. The improved thermal oxidative stability of silicone rubber by using iron oxide and carbon nanotubes as thermal resistant additives. Compos Sci Technol. 2013;76:52–60.
15. Zhang X, Zhang Q, Zheng J. Effect and mechanism of iron oxide modified carbon nanotubes on thermal oxidative stability of silicone rubber. Compos Sci Technol. 2014;99:1–7.
16. Diao S, Jin K, Yang Z, Lu H, Feng S, Zhang C. The effect of phenyl modified fumed silica on radiation resistance of silicone rubber. Mater Chem Phys. 2011;129:202–8.

17. Corrias M, Serp P, Kalck P, Dechambre G, Lacout JL, Castiglioni C, Kihn Y. High purity multiwalled carbon nanotubes under high pressure and high temperature. Carbon. 2003;41:2361–7.
18. Yi B, Rajagopalan R, Foley HC, Kim UJ, Liu X, Eklund PC. Catalytic polymerization and facile grafting of poly(furfuryl alcohol) to single-wall carbon nanotube: preparation of nanocomposite carbon. J Am Chem Soc. 2006;128:11307–13.
19. Qian WZ, Liu T, Wei F, Yuan HY. Quantitative Raman characterization of the mixed samples of the single and multi-wall carbon nanotubes. Carbon. 2003;41:1851–4.
20. Jia Y, Meng FL, Zhang MY, Guo Z, Chen X, Luo T, Fu XC, Kong LT, Liu JH, Huang XJ. Study on the interfacial structures of Tin oxide/multiwalled carbon nanotube heterojunctions. RSC Adv. 2012;2:1942–8.
21. Eder D, Windle AH. Morphology control of CNT–TiO_2 hybrid materials and rutile nanotubes. J Mater Chem. 2008;18:2036–43.
22. Hamdani S, Longuet C, Perrin D, Lopez-cuesta JM, Ganachaud F. Flame retardancy of silicone-based materials. Polym Degrad Stab. 2009;94:465–95.
23. Chen D, Nie J, Yi S, Wu W, Zhong Y, Liao J, Huang C. Thermal behaviour and mechanical properties of novel RTV silicone rubbers using divinyl-hexa [(trimethoxysilyl) ethyl]-POSS as cross-linker. Polym Degrad Stab. 2010;95:618–26.
24. Botter W, Ferreira Soares R, Galembeck F. Interfacial reactions and self-adhesion of polydimethylsiloxanes. J Adhes Sci Technol. 1992;6:791–805.
25. Sagar S, Iqbal N, Maqsood A, Shahid M, Shah NA, Jamil T, Bassyouni MI. Fabrication and thermal characteristics of functionalized carbon nanotubes impregnated polydimethylsiloxane nanocomposites. J Compos Mater. 2015;49:995–1006.
26. Sun K, Stroscio MA, Dutta M. Thermal conductivity of carbon nanotubes. J Appl Phys. 2009;105:074316.
27. Berber S, Kwon YK, Tománek D. Unusually high thermal conductivity of carbon nanotubes. Phys Rev Lett. 2000;84:4613–6.
28. Marosfői BB, Szabo A, Marosi G, Tabuani D, Camino G, Pagliari S. Thermal and spectroscopic characterization of polypropylene-carbon nanotube composites. J Therm Anal Calorim. 2006;86:669–73.
29. Zboril R, Mashlan M, Petridis D. Iron(III) oxides from thermal processes synthesis, structural and magnetic properties, Mössbauer spectroscopy characterization, and applications. Chem Mater. 2002;14:969–82.
30. Tronc E, Chaneac C, Jolivet JP. Structural and magnetic characterization of ε-Fe_2O_3. J Solid State Chem. 1998;139:93–104.
31. Watts PCP, Fearon PK, Hsu WK, Billingham NC, Kroto HW, Walton DRM. Carbon nanotubes as polymer antioxidants. J Mater Chem. 2003;13:491–5.
32. Hone J, Ellwood I, Muno M, Mizel A, Cohen ML, Zettl A, Smalley RE. Thermoelectric power of single-walled carbon nanotubes. Phys Rev Lett. 1998;80:1042.
33. Song SN, Wang XK, Chang RPH, Ketterson JB. Electronic properties of graphite nanotubules from galvanomagnetic effects. Phys Rev Lett. 1994;72:697.
34. Yu H, Quan X, Chen S. TiO_2-multiwalled carbon nanotube heterojunction arrays and their charge separation capability. J Phys Chem C. 2007;111:12987–91.
35. Kongkanand A, Kamat PV. Electron storage in single wall carbon nanotubes. Fermi level equilibration in semiconductor–SWCNT suspensions. ACS Nano. 2007;1:13–21.
36. Shi X, Jiang B, Wang J, Yang Y. Influence of wall number and surface functionalization of carbon nanotubes on their antioxidant behavior in high density polyethylene. Carbon. 2012;50:1005–13.